ARTICLE

Tensile Strain Capacity Prediction of Engineered Cementitious Composites (ECC) Using Soft Computing Techniques

Rabar H. Faraj[1,*], Hemn Unis Ahmed[2,3], Hardi Saadullah Fathullah[4], Alan Saeed Abdulrahman[2] and Farid Abed[5]

[1]Civil Engineering Department, University of Halabja, Halabja, Iraq

[2]University of Sulaimani, College of Engineering, Civil Engineering Department, Sulaimani, Iraq

[3]Civil Engineering Department, Komar University of Science and Technology, Sulaimani, Iraq

[4]Department of Engineering, Kurdistan Institution for Strategic Studies and Scientific Researches, Sulaimani, Iraq

[5]Department of Civil Engineering, American University of Sharjah, Sharjah, 26666, UAE

*Corresponding Author: Rabar H. Faraj. Email: rabar.faraj@uoh.edu.iq

ABSTRACT

Plain concrete is strong in compression but brittle in tension, having a low tensile strain capacity that can significantly degrade the long-term performance of concrete structures, even when steel reinforcing is present. In order to address these challenges, short polymer fibers are randomly dispersed in a cement-based matrix to form a highly ductile engineered cementitious composite (ECC). This material exhibits high ductility under tensile forces, with its tensile strain being several hundred times greater than conventional concrete. Since concrete is inherently weak in tension, the tensile strain capacity (TSC) has become one of the most extensively researched properties. As a result, developing a model to predict the TSC of the ECC and to optimize the mixture proportions becomes challenging. Meanwhile, the effort required for laboratory trial batches to determine the TSC is reduced. To achieve the research objectives, five distinct models, artificial neural network (ANN), nonlinear model (NLR), linear relationship model (LR), multi-logistic model (MLR), and M5P-tree model (M5P), are investigated and employed to predict the TSC of ECC mixtures containing fly ash. Data from 115 mixtures are gathered and analyzed to develop a new model. The input variables include mixture proportions, fiber length and diameter, and the time required for curing the various mixtures. The model's effectiveness is evaluated and verified based on statistical parameters such as R^2, mean absolute error (MAE), scatter index (SI), root mean squared error (RMSE), and objective function (OBJ) value. Consequently, the ANN model outperforms the others in predicting the TSC of the ECC, with RMSE, MAE, OBJ, SI, and R^2 values of 0.42%, 0.3%, 0.33%, 0.135%, and 0.98, respectively.

KEYWORDS

Engineered cementitious composites; fly ash; curing time; tensile strain capacity; modeling

Nomenclature

TSC	Tensile strain capacity
ECC	Engineered cementitious composite

ANN	Artificial neural network
LR	Linear relationship model
LR	Nonlinear model
MLR	Multi-logistic model
M5P	M5P-tree model
R^2	Coefficient of determination
MAE	Mean absolute error
RMSE	Root mean squared error
OBJ	Objective function
SI	Scatter index
FA	Fly ash
PP	Polypropylene
PE	Polyethylene
PVA	Polyvinyl alcohol
CS	Compressive strength
C	Cement
S	Sand
F	Fiber
SP	Superplasticizer
w/b	Water to binder ratio
MSS	Maximum size of sand
FL	Fiber length
FD	Fiber diameter
T	Curing time
SD	Standard deviation

1 Introduction

As one of the most economical and durable materials, concrete is extensively used in constructing various structures worldwide. To enhance the properties of this material and to make it more durable and robust, the construction industry, with the aid of researchers, continuously invests in developing its beneficial characteristics by introducing new materials and technologies. A remarkable result of this extensive research is the engineered cementitious composite (ECC), which has gained recognition for its high performance in the construction industry. Researchers have identified several weaknesses in plain concrete, including low tensile strength, brittleness, and low ultimate tensile strain. Addressing these deficiencies and introducing new materials have become significant research objectives. The fiber-reinforced high-performance material, known as engineered cementitious composite (ECC), developed by Li and his colleagues in 1992, is among the most effective alternatives to plain concrete [1–4]. The ECC's microstructure was optimized using micromechanical models to enhance ductility properties, reduce fracture widths to as low as 100 μm, and increase tensile strain capacity by 5% more than regular concrete [5].

ECC is preferred in various construction fields, such as retrofitting structures damaged by earthquakes, patching concrete pavements and slabs, and restoring dams due to its high strain capability, resistance against spalling, low micro-cracks, and high impermeability [6–10]. ECC is known for its high ductility, allowing it to deform significantly without fracturing or losing strength. This characteristic makes ECC well-suited for earthquake-resistant structures and other applications where toughness and durability are crucial. FRC, while stronger than plain concrete, is generally less

ductile than ECC. Additionally, ECC is highly crack-resistant because of its unique combination of high tensile strength and ductility. FRC also offers good crack resistance but might not perform as effectively as ECC in high-stress applications [11].

The ECC mixture typically consists of cement, fly ash, sand, water, and a chemical admixture with randomly scattered fibers. As indicated by [11], the proportions of the composting materials and their physical and chemical properties contribute to the design of the mixture. The types of fibers used in ECC production are generally polypropylene (PP), polyethylene (PE), and polyvinyl alcohol (PVA) composites. The rationale for using fiber in ECC is to enhance the tensile capacity of the material. Since PVA fiber possesses higher tensile strength than PP fiber, the flexural strength and toughness of ECC containing PVA fiber exceed that of ECC containing PP fiber [12]. The compressive strength of ECC is comparable to both ordinary and high-strength concretes. Due to its ductile property, as opposed to the brittleness of ordinary concrete, ECC is employed in a broad range of applications and has a promising future in various industries [13].

The compressive strength of concrete is a critical property when evaluating the overall quality of the material, leading other mechanical and durability parameters to be indirectly correlated with compressive strength [14,15]. For ECC, properties such as direct tensile strength and tensile strain capacity are more crucial to investigate. Several sets of specimens must be prepared, cured under various conditions, and tested to determine these properties for ECC. Concrete strength is often based on the 28-day strength capacity. Consequently, work might be halted until this point based on existing regulations, which can hinder project completion timelines and increase testing costs [16].

Determining the TSC of concrete without trials and preparing specimens has become one of the most challenging issues in construction material science [17], as the mixture proportion and component properties significantly affect the properties of ECC. With ongoing research on the TSC of ECC, the standard procedure for determining ECC characteristics may no longer be practical. Some researchers have derived regression models from the literature to link other ECC variables to its TSC. It is crucial to establish a simple, time-efficient procedure to predict experimental outcomes, especially since the TSC of ECC is highly sensitive to mixture proportions and various other variables. One potential solution could be soft computing approaches [18–20]. The primary advantage of this approach is its ability to offer solutions to both linear and nonlinear problems when mathematical models cannot demonstrate the relationships between central problem aspects [21,22].

Artificial intelligence systems have emerged as genuine tools for researchers studying cement-based composites to determine these materials' mechanical properties and provide the most effective methodologies. Machine learning has advanced as a potent method for gauging the structural and material performance of such materials [23]. An extensive set of actual data with features is required to make machine learning models more robust and inclusive. Cavaleri et al. [23] proposed ensemble algorithms for predicting the bond strength of corroded reinforced concrete. They found that the models accurately depict the nonlinear behavior of corroded reinforced concrete. Another study used the M5P model tree to assess the dynamic modulus of asphalt concrete [24]. Ahmed et al. [25] adapted three standard models, linear, nonlinear, and multi-logistic regression, to predict the compressive strength (CS) of fly ash-based geopolymer concrete, using twelve actual mixture proportions and curing methods as model inputs. Moreover, the impact of the molarity of NaOH, nano-silica content, the ratio of sodium hydroxide to sodium silicate, the binder content, the aggregate amount, and the age of CS in the geopolymer concrete was investigated, and five distinct models, including the ANN and M5P tree, were developed to predict and estimate CS in the composites. Due to the limitations of soft computing models in predicting ECC characteristics, another effort was made by [26,27] to forecast

the compressive and tensile strengths of ECC mixtures. This research developed an ANN model using data from 79 experiments and 12 input parameters from existing literature. The results underscored the ANN model's efficacy in estimating the compressive and tensile strengths of ECC that includes PVA fiber in its composition. Since prior research in this area was deemed insufficient, the present study utilized five different ML models and ten input parameters to predict ECC's TSC.

Since ECCs are commonly used in structural applications where ductility is paramount, there are few studies on estimating the TSC of ECCs with fly ash, complicating their efficient use in construction. Additionally, the building industry increasingly seeks novel building materials with unique properties to extend the longevity of concrete structures. This necessitates the creation of new models to anticipate the behavior and properties of these materials. The primary aim of this study is to explore the effects of various mixture proportions, such as cement (C), fly ash (FA), sand (S), fiber (F), w/b ratio, and superplasticizer (SP), on the TSC of ECC mixtures over both short (3 days) and long (90 days) durations. Extensive experimental data from 115 specimens, combined with diverse modeling approaches, were employed to achieve the following objectives: (i) examine the influence of cement, fly ash, sand, fibers, and SP contents, along with curing time, w/c ratio, maximum aggregate size, fiber length, and diameter, on the TSC of eco-friendly ECC containing fly ash, (ii) enable the construction industry to use the model for estimating ECC's TSC without additional laboratory tests and analysis, (iii) confirm the model's reliability compared to others (ANN, nonlinear, linear, and multi-logistic relation models) in terms of TSC prediction accuracy for sustainable ECC with fly ash. Moreover, an essential goal of this research is to develop mathematical models to predict the TSC of a novel composite type (ECC with fly ash) and leverage the model's benefits in the construction sector.

2 Methodology

Data from various previous studies were collected to achieve the objectives of this research, totaling 115 datasets. These datasets were entered into an Excel sheet, after which they were arranged, divided, and statistically analyzed. The data were then randomly distributed and separated into two groups: the major group, which constituted 70% of the data, was used to generate the models and is referred to as training data, while the remaining 30% of the data was used to test the generated models [17,28].

The TSC of the ECC composites produced with different mix proportions and fly ash contents has been collected and presented in Table 1. This table encompasses most previous studies on this topic, particularly those that examined the effect of the composting material proportion on the properties of the ECC. The test results, including the fundamental parameters presented in Table 1, were used to predict the TCS of ECC using different approaches previously mentioned and compared to the reported measured TCS%. The workflow is illustrated in Fig. 1.

Table 1: Summary of the constitutes of ECC mixes reported in the literature

Ref.	Cement content (kg/m³)	Fly ash content (kg/m³)	w/b	Sand		SP content (kg/m³)	Fiber			Age (day)	Tensile strain capacity (%) (TSC)
				Max. size (μm)	Content (kg/m³)		Content (kg/m³)	Length (mm)	Diameter (μm)		
[29]	375	825	0.26	200	432	5.52	26	12	39	28	2.9
	375	825	0.26	200	432	5.04	26	12	39	28	2.8
	375	825	0.26	425	432	4.8	26	12	39	28	2.4
	375	825	0.26	600	432	4.44	26	12	39	28	1.5
	222	978	0.26	200	432	5.04	26	12	39	28	4.1
	222	978	0.26	425	432	4.8	26	12	39	28	4.2
	222	978	0.26	425	432	5.04	26	12	39	28	4.7
	375	825	0.26	425	432	5.16	26	12	39	28	3.2
[30]	472	755	0.27	300	444	10.8	26	8	39	28	1.8
	472	755	0.27	300	444	10.8	26	12	39	28	2
[31]	570	684	0.3	300	455	5.7	28.6	12	39	28	0.77
[32]	570	684	0.56	250	456	6.84	29	8	39	28	2.9
	570	684	0.56	250	456	6.84	29	8	39	28	3.6
[33]	232	1019	0.26	250	450	4.3	26	12	39		2.68
[34]	382	890	0.25	250	462	15.3	26	8	40	28	3.2
	382	763	0.25	250	462	15.3	26	8	40	28	3.76
	382	636	0.25	250	462	15.3	26	8	40	28	3.56
	382	509	0.25	250	462	15.3	26	8	40	28	3.36
	382	890	0.25	250	462	15.3	26	8	40	90	2.79
	382	763	0.25	250	462	15.3	26	8	40	90	3.28
	382	636	0.25	250	462	15.3	26	8	40	90	3.3
	382	509	0.25	250	462	15.3	26	8	40	90	2.51
[11]	936	201	0.32	250	601	4.2	26	8	39	56	6
[35]	393	865	0.25	250	457	5	26	12	39	28	2
[36]	393	865	0.25	250	457	5	26	12	39	28	4.2
[37]	570	684	0.27	250	454	5	16.9	12	39	3	3.22
	337	912	0.27	250	454	2.5	16.9	12	39	3	3.28
	570	684	0.27	250	454	5	16.9	12	39	7	3.03
	337	912	0.27	250	454	2.5	16.9	12	39	7	3.1
	570	684	0.27	250	454	5	16.9	12	39	28	2.7
	337	912	0.27	250	454	2.5	16.9	12	39	28	3.57
	570	684	0.27	250	454	5	16.9	12	39	56	2.33
	337	912	0.27	250	454	2.5	16.9	12	39	56	3.27
	570	684	0.27	250	454	5	16.9	12	39	90	2.2
	337	912	0.27	250	454	2.5	16.9	12	39	90	3.07
[38]	578	694	0.25	200	462	7.51	26	12	39	28	3
[39,40]	570	684	0.23	150	454	5.3	26	8	40	28	2.8
[41,42]	570	684	0.27	200	455	4.9	26	8	39	7	3.48
	570	684	0.27	200	455	4.9	26	8	39	28	3.16
[43,44]	570	684	0.27	200	455	4.9	26	8	39	7	3.48
	386	847	0.27	200	448	3.7	26	8	39	7	4.21
	570	684	0.27	200	455	4.9	26	8	39	28	3.16
	386	847	0.27	200	448	3.7	26	8	39	28	3.4

Table 1 (continued)

Ref.	Cement content (kg/m³)	Fly ash content (kg/m³)	w/b	Sand		SP content (kg/m³)	Fiber			Age (day)	Tensile strain capacity (%) (TSC)
				Max. size (μm)	Content (kg/m³)		Content (kg/m³)	Length (mm)	Diameter (μm)		
[45]	570	684	0.27	200	455	5.1	26	8	39	7	3.9
	570	684	0.27	200	455	5.1	26	8	39	28	3.1
	558	669	0.27	200	446	2.3	26	8	39	14	2.91
[46,47]	375	823	0.27	200	435	2	26	8	39	14	3.24
	558	669	0.27	200	446	2.3	26	8	39	28	2.73
	375	823	0.27	200	435	2	26	8	39	28	3.02
	838	0	0.43	250	838	17	26	12	39	28	4.88
[48]	583	700	0.23	250	467	19	26	12	39	28	3.41
	318	701	0.28	250	701	19	26	12	39	28	3.9
	571	685	0.25	250	456	6.8	26	8	39	3	4.6
	477	763	0.25	250	456	6.05	26	8	39	3	4.2
	412	824	0.25	250	456	5.52	26	8	39	3	4.1
	362	870	0.25	250	456	5.1	26	8	39	3	4.3
	324	906	0.25	250	456	5.29	26	8	39	3	4.4
	292	965	0.25	250	456	5.1	26	8	39	3	4.3
	266	959	0.25	250	456	5.8	26	8	39	3	4
	190	1063	0.25	250	456	6.45	26	8	39	3	3.8
	571	685	0.25	250	456	6.8	26	8	39	28	2.7
	477	763	0.25	250	456	6.05	26	8	39	28	3.7
	412	824	0.25	250	456	5.52	26	8	39	28	3
	362	870	0.25	250	456	5.1	26	8	39	28	2.9
	324	906	0.25	250	456	5.29	26	8	39	28	3
	292	965	0.25	250	456	5.1	26	8	39	28	2.7
[49]	266	959	0.25	250	456	5.8	26	8	39	28	2.5
	190	1063	0.25	250	456	6.45	26	8	39	28	3.3
	571	685	0.25	250	456	6.8	26	8	39	90	1.8
	477	763	0.25	250	456	6.05	26	8	39	90	3
	412	824	0.25	250	456	5.52	26	8	39	90	3.1
	362	870	0.25	250	456	5.1	26	8	39	90	2.3
	324	906	0.25	250	456	5.29	26	8	39	90	3.3
	292	965	0.25	250	456	5.1	26	8	39	90	2.9
	266	959	0.25	250	456	5.8	26	8	39	90	2.6
	190	1063	0.25	250	456	6.45	26	8	39	90	3.4
	636	636	0.25	250	462	17.4	26	8	40	28	1.8
	636	636	0.25	250	462	17.4	26	8	40	28	2.22
[50]	636	636	0.25	250	462	17.4	26	8	40	28	2.46
	382	890	0.25	250	462	16	26	8	40	28	2.5
	382	890	0.25	250	462	16	26	8	40	28	3
	382	890	0.25	250	462	16	26	8	40	28	3.12
	418	836	0.19	600	456	5.7	26	8	39	28	4.5
[51]	570	684	0.25	600	456	5.7	26	8	39	28	4.25
	418	836	0.22	600	456	7.41	26	8	39	28	4
	404	605	0.24	4750	756	23	19	12	24	28	4.09
	450	673	0.24	4750	617	17	19	12	24	28	9.07
	502	753	0.24	4750	452	11	19	12	24	28	10.12
	493	739	0.27	4750	437	8	19	12	24	28	8.74
	484	726	0.3	4750	435	6	19	12	24	28	9.43

(Continued)

Table 1 (continued)

Ref.	Cement content (kg/m³)	Fly ash content (kg/m³)	w/b	Sand		SP content (kg/m³)	Fiber			Age (day)	Tensile strain capacity (%) (TSC)
				Max. size (μm)	Content (kg/m³)		Content (kg/m³)	Length (mm)	Diameter (μm)		
	404	605	0.24	2360	756	20	19	12	24	28	4.07
	450	673	0.24	2360	617	15	19	12	24	28	7.45
[52]	502	753	0.24	2360	452	10	19	12	24	28	9.44
	493	739	0.27	2360	437	8	19	12	24	28	10.39
	484	726	0.3	2360	435	6	19	12	24	28	9.54
	404	605	0.24	212	756	20	19	12	24	28	6.47
	450	673	0.24	212	617	15	19	12	24	28	9.95
	502	753	0.24	212	452	10	19	12	24	28	10.75
	493	739	0.27	212	437	8	19	12	24	28	9.21
	484	726	0.3	212	435	6	19	12	24	28	8.12
[31,53]	570	684	0.3	300	456	5.1	28.6	12	39	28	0.77
	570	684	0.3	300	456	6.77	17	12	26	28	0.33
	448	807	0.3	300	456	6.5	17	12	26	28	0.48
	368	886	0.3	300	456	6.27	17	12	26	28	0.51
	314	941	0.3	300	456	6	17	12	26	28	0.71
	273	981	0.3	300	456	5.89	17	12	26	28	0.6
	447	807	0.28	300	456	10.4	17	12	26	28	0.17
	447	807	0.32	300	456	5.643	17	12	26	28	0.5
	368	886	0.28	300	456	10	17	12	26	28	0.28
	368	886	0.32	300	456	5.26	17	12	26	28	0.52
	314	941	0.28	300	456	9.78	17	12	26	28	0.32
[10]	314	941	0.32	300	456	5	17	12	26	28	0.42
	368	886	0.3	300	380	6.27	17	12	26	28	0.65
	368	886	0.3	300	532	6.27	17	12	26	28	0.16
	447	807	0.3	300	456	2.5	0	12	26	28	0.02
	447	807	0.3	300	456	6.27	15.6	12	26	28	0.29
	447	807	0.3	300	456	6.77	18.2	12	26	28	0.44
	368	886	0.28	300	456	3.63	21	12	39	28	2.37
	368	886	0.26	300	456	4	21	12	39	28	2.01
	368	886	0.28	300	456	2.5	13	12	39	28	1.57
	368	886	0.28	300	456	3.13	21	12	39	28	2.76
	368	886	0.28	300	456	3.5	26	12	39	28	4.25
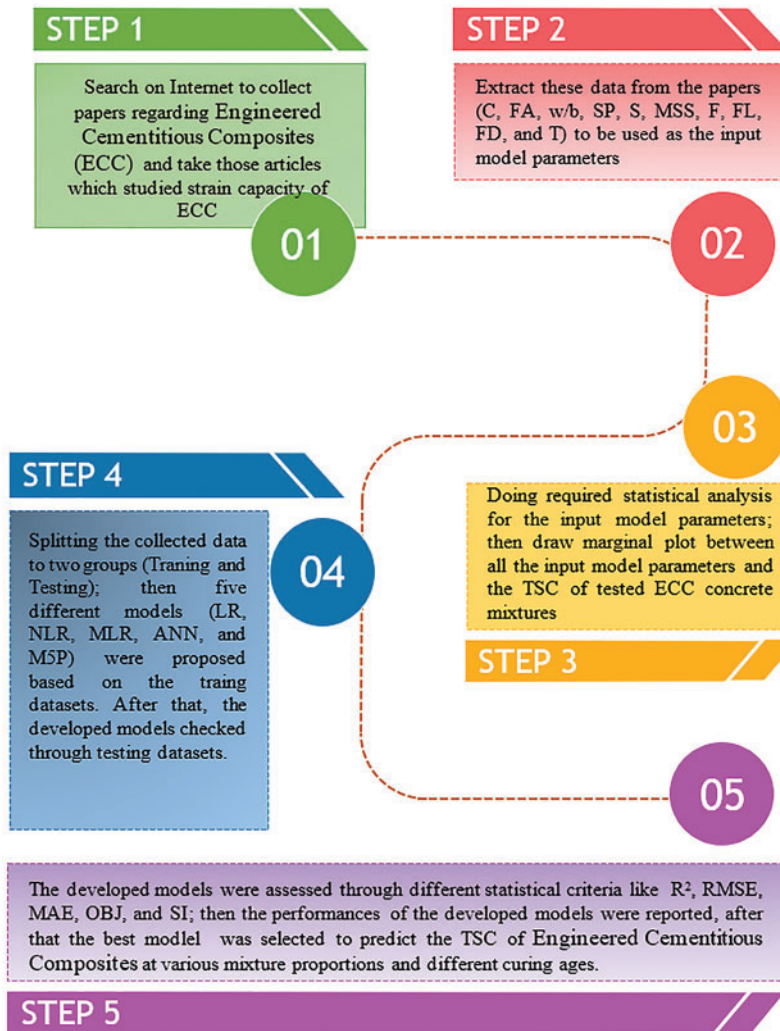
Figure 1: The research methodology in terms of a flow chart diagram

3 Statistical Evaluation

At this stage of the study, the relationships between the dependent and independent variables were investigated to determine the strength of the association between them and with the TSC of ECC. The relationships of cement content, fly ash content, w/b ratio, maximum aggregate size (sand), sand content, SP content, fiber (content, diameter, and length), and curing time were plotted against the empirical direct tensile strain as depicted in Figs. 2a–2j successively. A normal distribution of TSC from previous research was illustrated in Fig. 3. To demonstrate the distribution of each variable and its relationship with the TSC, statistical functions such as standard deviation (SD), skewness, variance, minimum, average, maximum, and kurtosis were calculated and summarized in Table 2. As derived from the literature, the properties and behavior of ECC, especially TSD, are significantly influenced by the length and diameter of the fibers used in their structure. Based on this data, fiber length, diameter, and fiber content were all considered as input variables.

Figure 2: (Continued)

(d)

(e)

(f)
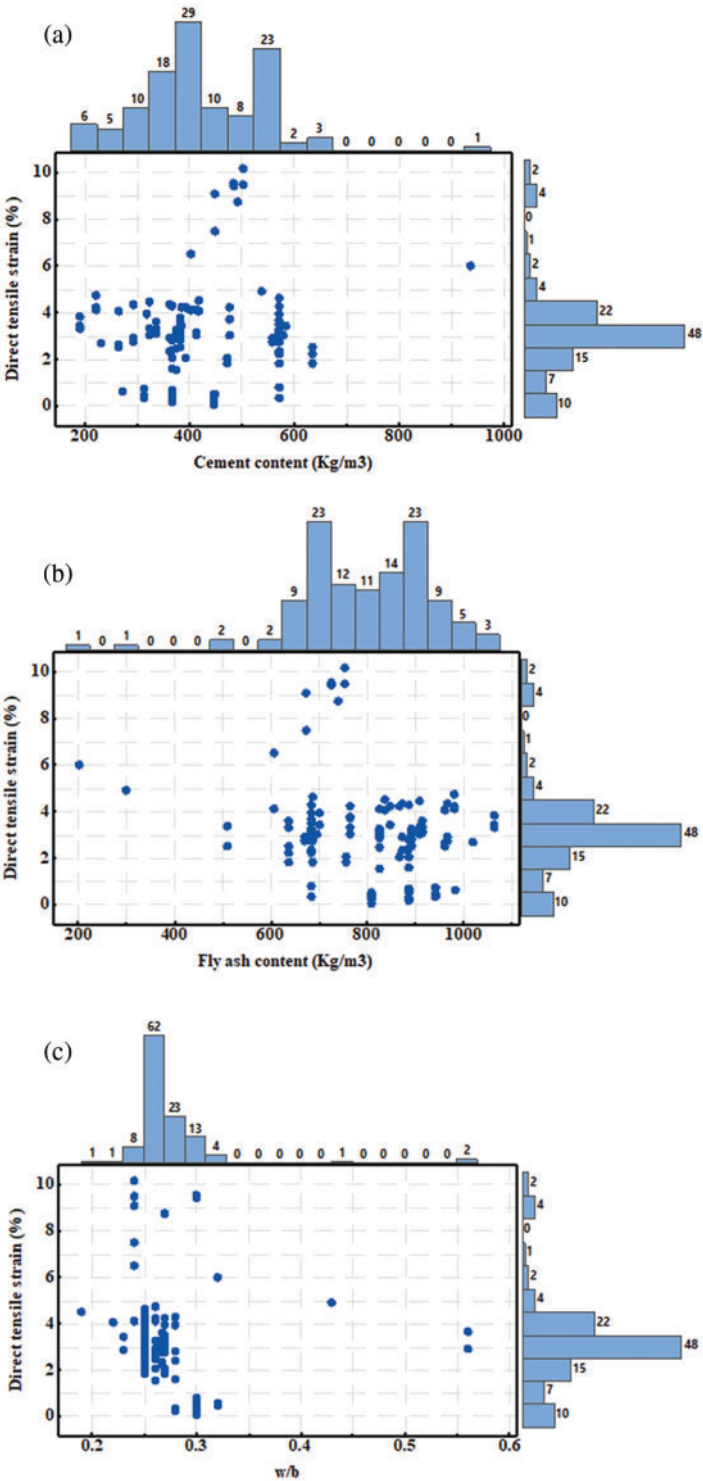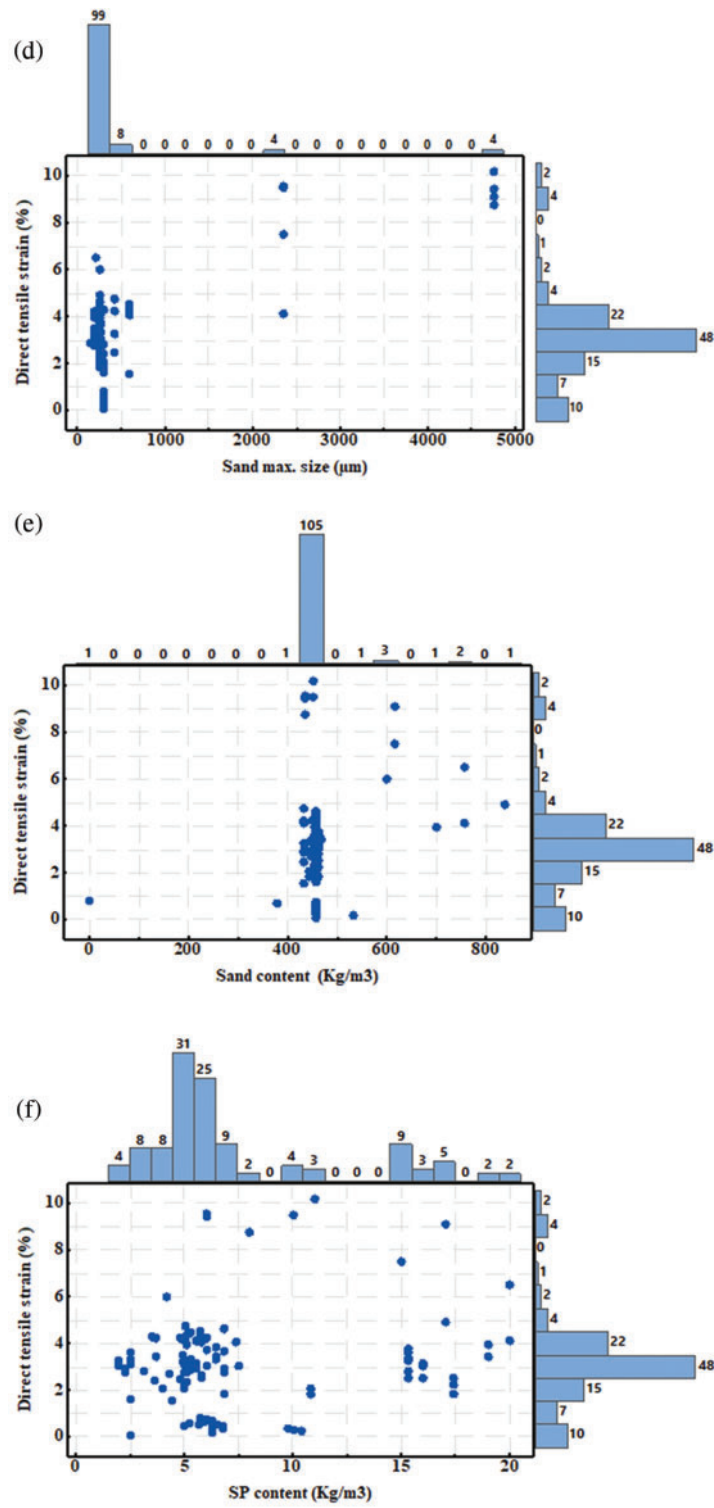
Figure 2: (Continued)
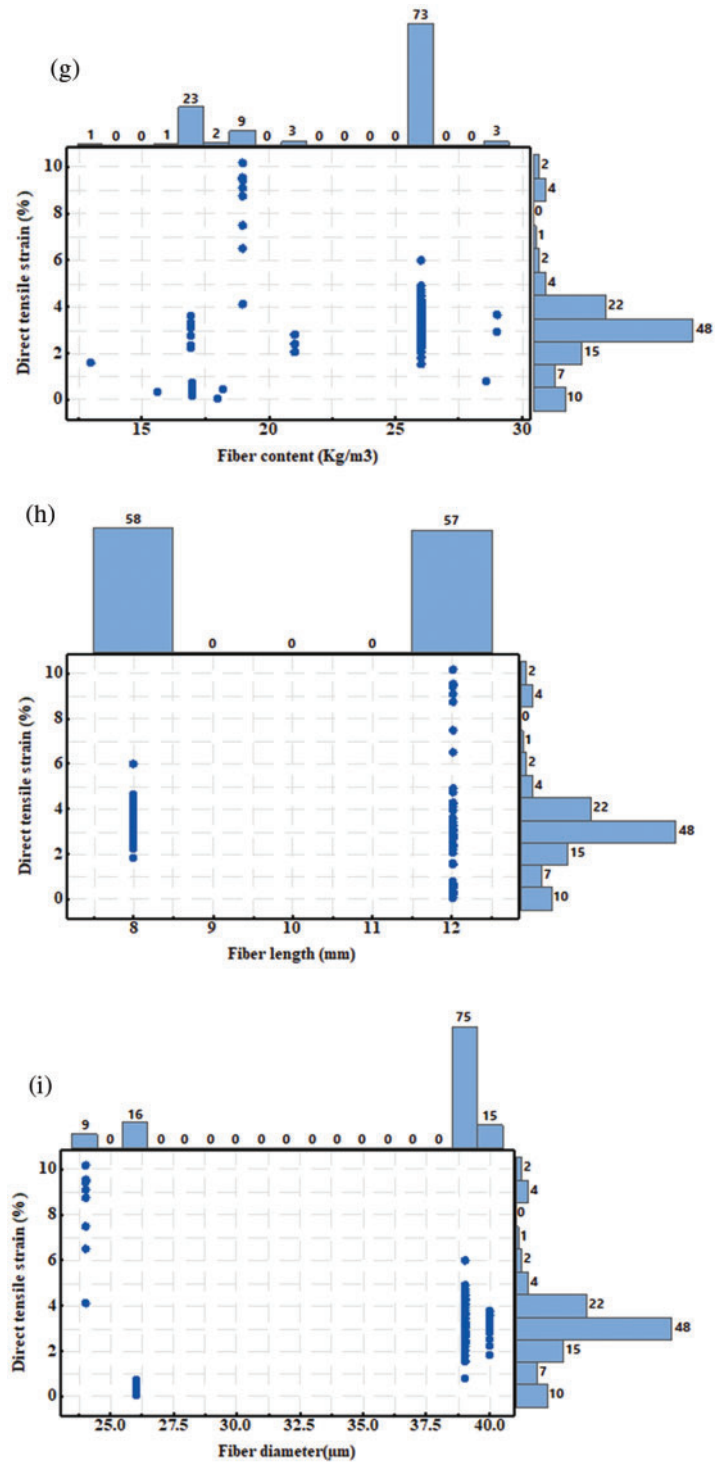
Figure 2: (Continued)
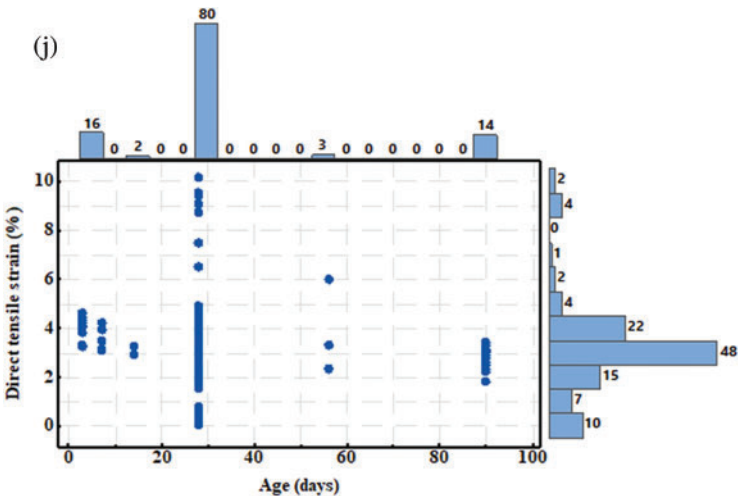
Figure 2: Marginal plot for the TSC of ECC *vs.* (a) cement content; (b) fly ash content; (c) w/b; (d) sand maximum size; (e) sand content; (f) superplasticizer content; (g) fiber content; (h) fiber length; (i) fiber diameter; (j) specimens ages
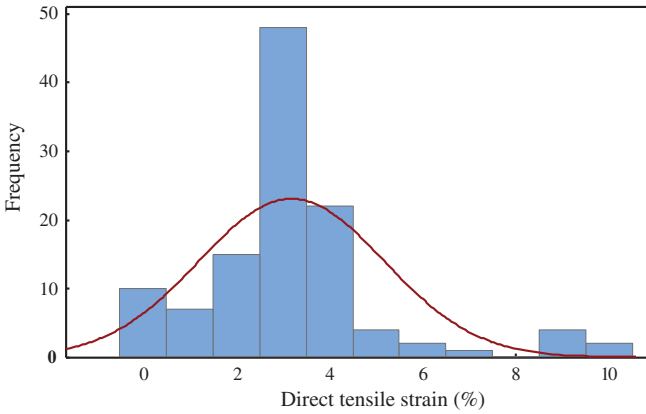
Figure 3: The TSC histogram of the gathered datasets at various curing ages

Generally, the fibers used in previous research were of the PVA type with lengths and diameters of 6–12 mm and 12–40 μm, respectively. The contents of these fibers ranged from 4.55 to 39 kg/m^3. The type of cement used in most prior studies was OPC, adhering to the specifications of ASTM C 150 with fineness values between 300 and 400 m^2/kg and a specific gravity ranging from 3.05 to 3.20. The type of fly ash used as a cement replacement was Class-F, with contents ranging from 201 to 1150 kg/m^3. Sand contents were between 380 and 756 kg/m^3, with maximum sizes of 100–4750 μm. The superplasticizer employed in the ECC mixture from previous research was polycarboxylate-based, possessing high water-reducing capabilities to minimize water content and enhance workability.

Table 2: A summary of the statistical analysis of the model's input parameters

Model parameters	No. of data	Average	Median	St. Div.	Min.	Max.	Variance	Skewness	Kurtosis
Cement content (Kg/m^3)	115	424.71	386	119.89	190	936	14372.90	0.67	1.65
Fly ash content (Kg/m^3)	115	795.55	823	139.87	201	1063	19562.78	−0.97	2.72
w/b	115	0.27	0.26	0.05	0.19	0.56	0.00	4.49	25.02
Sand max. size (μm)	115	500.45	250	899.90	150	4750	809814.21	4.06	15.99
Sand content (Kg/m^3)	115	464.21	456	77.14	0.36	838	5950.38	0.47	19.11
SP content (Kg/m^3)	115	7.53	5.7	4.72	2	20	22.24	1.29	0.41
Fiber content (Kg/m^3)	115	23.25	26	4.14	13	29	17.12	−0.78	−1.12
Fiber length (mm)	115	9.98	8	2.01	8	12	4.03	0.02	−2.04
Fiber diameter(μm)	115	36.15	39	5.78	24	40	33.41	−1.40	0.02
Age (days)	115	32.77	28	23.48	3	90	551.27	1.57	1.84
TSC (%)	115	3.19	3.07	1.99	0.02	10.12	3.95	1.39	3.29

4 Modeling

From the literature and the results of the analysis in Section 3, it is clear that a direct relationship between the TSC of ECC and its individual constituents is not available. Therefore, all ingredients could be combined and incorporated into a single model to determine the influence of each parameter on the TSC. Consequently, five distinct soft-computing techniques were proposed, as explained below.

4.1 Linear Relationship Model (LR)

As previously mentioned, this research aims to incorporate as many variables as possible that are strongly related to the TSC of ECC into a model. The linear regression model is a common tool used to evaluate the compressive strength of ECC [54], as represented in Eq. (1).

$$\sigma_c = \alpha 1 + \alpha 2(w/c) \tag{1}$$

where $\alpha 1$ and $\alpha 2$ are coefficients; w/c is the significant parameter of the model that influences the compressive strength of concrete. This model has not considered the influence of other contributing parameters, such as curing time, on ECC behavior. The sum of squared errors and the least squares approach, implemented using the Excel program with the solver feature, were used to compute the value of each parameter in the current model. As a result, Eq. (2) was developed to include most factors influencing the tensile strain capacity.

$$TSC = \alpha 1 + \alpha 2\,(C) + \alpha 3\,(FA) + \alpha 4\left(\frac{w}{b}\right) + \alpha 5\,(SMS) + \alpha 6\,(S) + \alpha 7\,(SP) + \alpha 8\,(F)$$
$$+ \alpha 9\,(FL) + \alpha 10\,(FD) + \alpha 11\,(A) \tag{2}$$

where TSC = Tensile Starin Capacity, C = Cement content (kg/m³), FA = Fly ash content (kg/m³), w/b = Water to Binder ratio, MSS = The maximum size of sand (μm), S = Sand content (kg/m³), SP = Superplasticizer dosage (kg/m³), F = Fiber content (kg/m³), FL = Fiber length (mm), FD = Fiber diameter (μm).

where $\alpha 1, \alpha 2, \alpha 3, \alpha 4, \alpha 5, \alpha 6, \alpha 7, \alpha 8, \alpha 9, \alpha 10$, and $\alpha 11$ are the model parameters. Since the changes in the factors are linear, Eq. (2) can be utilized to replace Eq. (1). Many factors affect the TSC and interact with one another, but this is not necessarily the case. Subsequently, the model should be updated frequently for a better prediction of the compressive strength [54,55].

4.2 NLR Model

The relationship between different variables of Eqs. (1) and (2) can be generated as stated in Eq. (3); from this, the TSC of ordinary ECC and ECC incorporated flay ash can be predicted. Eq. (3) can efficiently be used to design NLR [56,57].

$$TSC = \alpha 1 * (C)^{\alpha 2} * \left(\frac{w}{b}\right)^{\alpha 3} * (SMS)^{\alpha 4} * (S)^{\alpha 5} * (SP)^{\alpha 6} * (F)^{\alpha 7} * (FL)^{\alpha 8} * (FD)^{\alpha 9} * (A)^{\alpha 10} + \alpha 11$$

$$* (C)^{\alpha 12} * \left(\frac{w}{b}\right)^{\alpha 13} * (SMS)^{\alpha 14} * (S)^{\alpha 15} * (SP)^{\alpha 16} * (F)^{\alpha 17} * (FL)^{\alpha 18} * (FD)^{\alpha 19} * (A)^{\alpha 20} * (FA)^{\alpha 21} \qquad (3)$$

Similar to the LR model, the sum of error squares and the least square approach were determined using the Excel solver. The abbreviations in the equation are identical to those for the LR model.

4.3 MLR Model

When the expected variables contain a parameter higher than two stages, the use of MLR, a statistical method similar to a multiple linear regression model, can be used [58]. Eq. (4) is utilized to calculate variance among predictable and independent variables.

$$TSC = \alpha 1 * (C)^{\alpha 2} * (FA)^{\alpha 3} * \left(\frac{w}{b}\right)^{\alpha 4} * (SMS)^{\alpha 5} * (S)^{\alpha 6} * (SP)^{\alpha 7} * (F)^{\alpha 8} * (FL)^{\alpha 9} * (FD)^{\alpha 10} * (A)^{\alpha 11} \qquad (4)$$

The disadvantage of this equation is its inadequacy to predict the TSC of ECCs, not including FA. Using this equation, the fly ash or other ingredient contents should be greater than zero.

4.4 ANN Model

The Weka software package (version 3.8.5) was used for ML predictions [59]. The ANN is the inverse of the forward neural network [55,60,61]. The model consists of three distinct layers: input, output, and hidden layers. The input layer receives the signal to be investigated, and the output layer presents the results of fundamental tasks such as classification and prediction. In the computational ANN engine, an infinite number of hidden layers exist between the input and output layers. Similarly to a feed-forward network, data transfer occurs from the source to the target layer in the ANN engine. Multiple hidden layers were refined over trial cycles to determine the most appropriate number of hidden layers for error reduction and R^2 [62]. To establish an optimal network topology, the derived ANN model was evaluated for various layers using both projected TSC and actual measured TSC of ECCs to achieve the best fit between them.

It was determined that the ANN structure composed of one hidden layer and seven neurons (Fig. 4) was the best-performing network with the highest R^2 and lowest MAE and RMSE (as shown in Fig. 5). Eqs. (5)–(7) provide the ANN model's general equations [63].

From linear node 0:

$$\sigma_c = Threshold + \left(\frac{Node\ 1}{1 + e^{-B1}}\right) + \left(\frac{Node\ 2}{1 + e^{-B2}}\right) + \ldots \qquad (5)$$

From sigmoid node 1:

$$B1 = Threshold + \sum (Attribute * Variable) \qquad (6)$$

From sigmoid node 2:

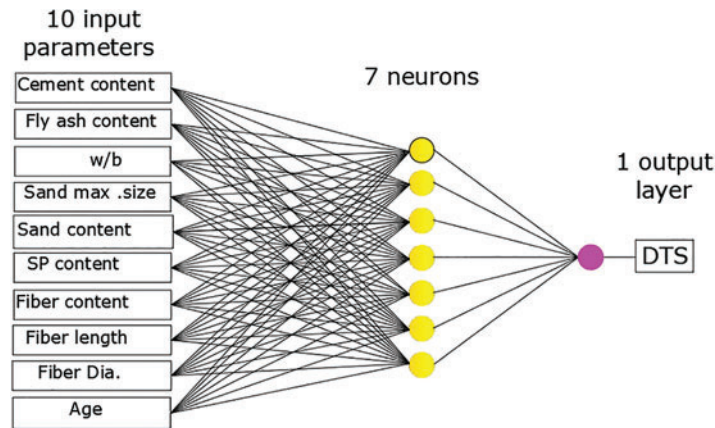$$B2 = Threshold + \sum (Attribute * Variable) \qquad (7)$$

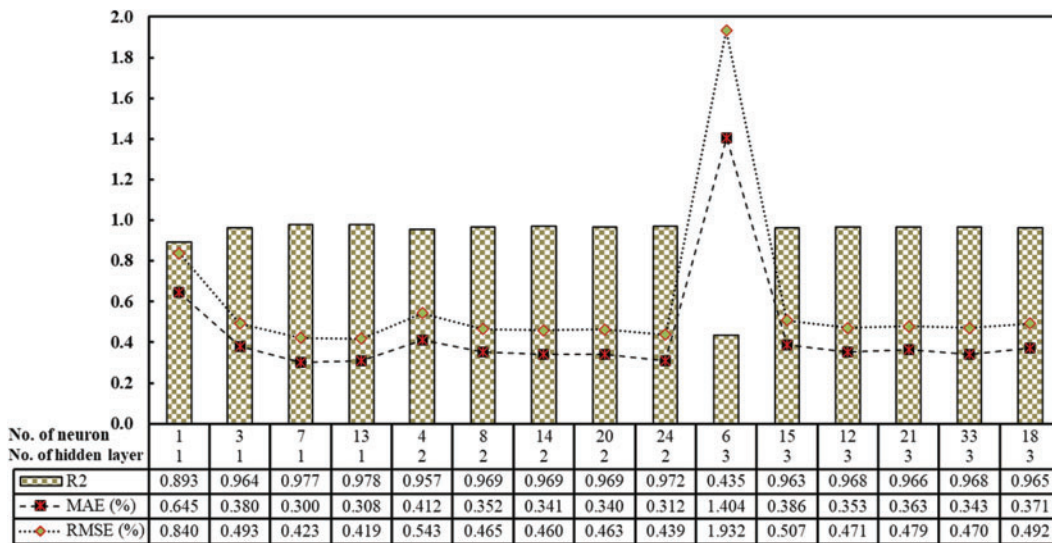**Figure 4:** ANN model optimal network architecture

Figure 5: Choose the best-hidden layer and neurons for an ANN model based on the model's R^2, MAE, and RMSE performances

4.5 M5P-Tree Model (M5P)

The modified version of the Quinlan M5 technique is referred to as the M5P-tree [64,65]. The key advantage of this model is its ability to handle a vast amount of data efficiently across countless attributes and dimensions. The nodes in the M5P tree display both error estimates and information on tree division criteria. The evaluation of any function linked to a specific node is determined by the feature that significantly reduces the anticipated error. The tree-division criteria of the M5P-tree model are derived from the error estimates at the node levels. The M5P-tree error represents the standard deviation of a node's class value. The division of nodes is guided by the feature that minimizes the projected error after analyzing each attribute. Due to the model's branching structure, the smaller nodes (sub-trees) possess a lower standard deviation than others. Once all potential structures are evaluated, the parent nodes (larger nodes) reflect the structure with the highest likelihood of error

reduction. This partitioning also leads to the formation of a vast tree-like structure, which can promote overfitting.

As shown below, the general equation of the M5P-tree model is similar to the linear regression equation–Eq. (8).

$$TSC = \alpha 1 + \alpha 2\,(C) + \alpha 3\,(FA) + \alpha 4\left(\frac{w}{b}\right) + \alpha 5\,(SMS) + \alpha 6\,(S) + \alpha 7\,(SP) + \alpha 8\,(F) + \alpha 9\,(FL)$$
$$+ \alpha 10\,(FD) + \alpha 11\,(A) \tag{8}$$

4.6 Assessment Criteria for the Developed Models

With the help of several assessment tools, namely the coefficient of determination (R^2), the Scatter Index (SI), the OBJ, the RMSE, and the MAE, the efficiency of the proposed models was evaluated. The following equations are suitable for this evaluation:

$$R^2 = \left(\frac{\sum_{p=1}^{p}\left(t_p - t'\right)\left(y_p - y'\right)}{\sqrt{\left[\sum_{p=1}^{p}\left(t_p - t'\right)^2\right]\left[\sum_{p=1}^{p}\left(y_p - y'\right)^2\right]}}\right)^2 \tag{9}$$

$$RMSE = \sqrt{\frac{\sum_{p=1}^{p}(y_p - t_p)^2}{p}} \tag{10}$$

$$MAE = \frac{\sum_{p=1}^{p}|(y_p - t_p)|}{p} \tag{11}$$

$$SI = \frac{RMSE}{t'} \tag{12}$$

$$OBJ = \left(\frac{n_{tr}}{n_{all}} * \frac{RMSE_{tr} + MAE_{tr}}{R_{tr}^2 + 1}\right) + \left(\frac{n_{tst}}{n_{all}} * \frac{RMSE_{tst} + MAE_{tst}}{R_{tst}^2 + 1}\right) \tag{13}$$

where yp = Predicted route pattern, tp = Actual route pattern, T = The mean of the actual value, y' = The mean of the projected value, tst = Tested dataset, n = No. of patterns (collected data) in the link dataset, tr = Trained dataset.

The indications of SI parameter for the performance are as follows [66,67]:

> 0.3 = Performance is Poor

$0.2–0.3$ = Performance is Fair

$0.1–0.2$ = Performance is Well

< 0.1 = Performance is Excelent

5 Analysis and Output

5.1 The LR Model

The relationship between measured and predicted TSC of ECC for both training and testing samples is depicted in Figs. 6a and 6b. By optimizing the sum of error squares and least square methods, the value of each parameter in the existing model was calculated.
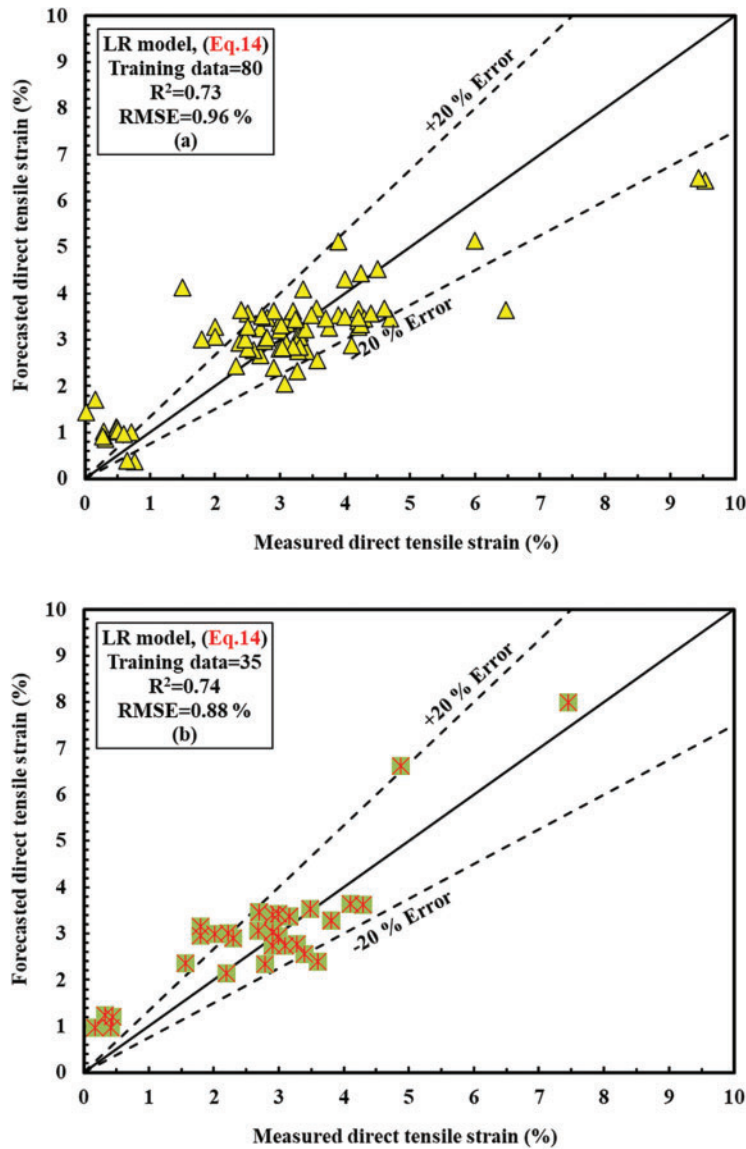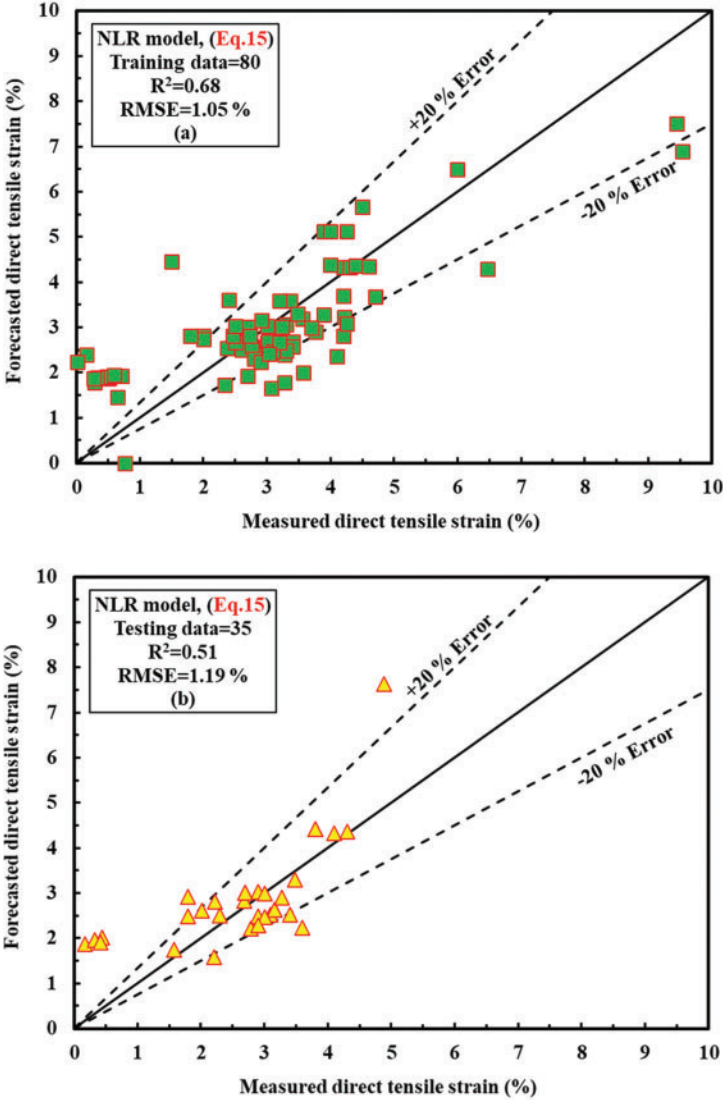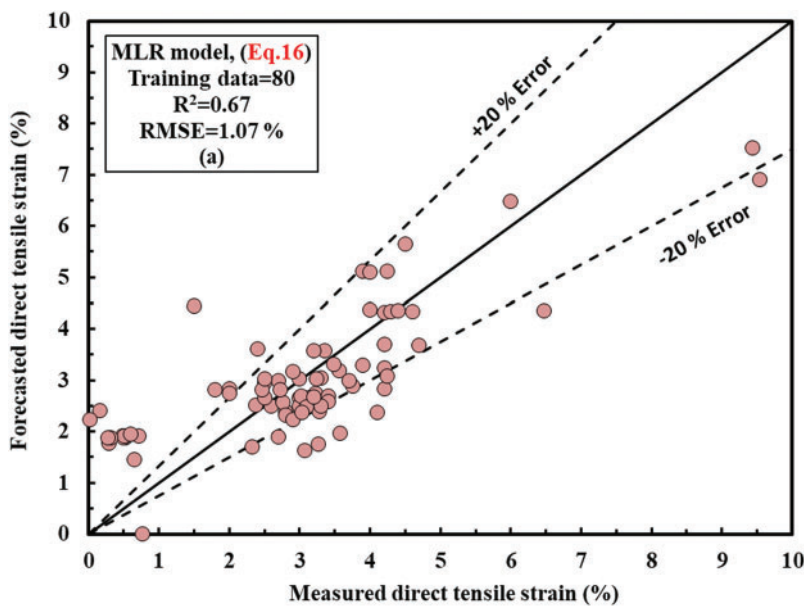
Figure 6: Comparison of the TSC of ECC mixtures that were tested and the TSC that the LR model predicted; (a) training datasets; (b) testing datasets

According to this model, the TSC of ECC-incorporated fly ash was significantly influenced by the w/b ratio and the diameter of the fiber content. The LR model with different weighted parameters is presented in Eq. (14).

$$TSC = -1.88 - 0.002\,(C) - 0.003\,(FA) - 4.214\left(\frac{w}{b}\right) + 0.002\,(SMS) + 0.009\,(S) - 0.059\,(SP)$$

$$+ 0.08\,(F) - 0.026\,(FL) + 0.102\,(FD) - 0.008\,(A) \tag{14}$$

From the equation above, it is evident that the w/b ratio greatly influences the TSC. This observation aligns with empirical findings in the literature. The assessment parameters R^2, RMSE,

and MAE were 0.73, 0.96%, and 0.7%, respectively. Moreover, the OBJ and SI values for the training datasets were 0.94% and 0.308.

5.2 NLR Model

Using data from the literature, the relationship between predicted and actual TSC of ECC incorporating fly ash for both training and testing datasets is shown in Figs. 7a and 7b. It was established that the maximum size of sand content, fiber concentration, and fiber diameter are the most influential parameters on the CS of ECC mixtures, as substantiated by an extensive set of experiments noted in Table 1. Adjusting the fiber amount and increasing the maximum sand content size significantly impacted the CS of ECC incorporating fly ash.
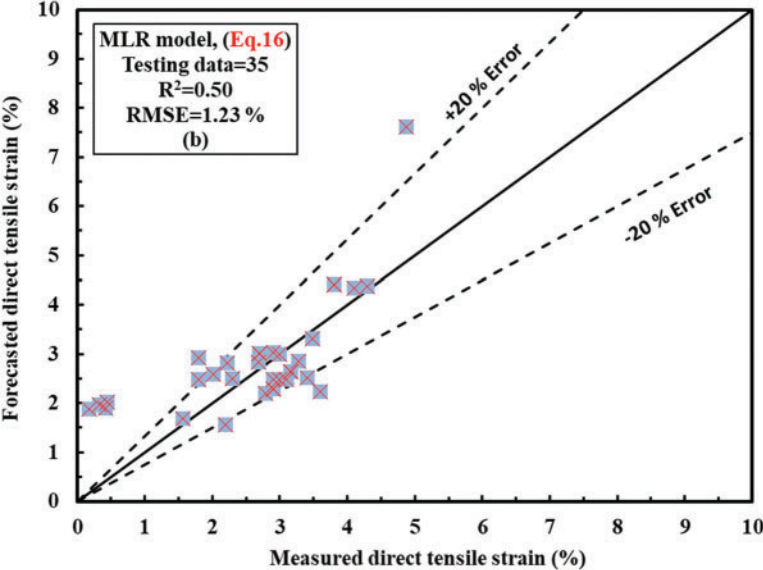

Figure 7: Comparison of the TSC of ECC mixtures that were tested and the TSC that the NLR model predicted; (a) training datasets; (b) testing datasets

The following equation is the suggested model for the NLR model with different variable parameters (Eq. (15)):

$$TSC = -4269895 * (C)^{0.606} * \left(\frac{w}{b}\right)^{1.57} * (SMS)^{-4.42} * (S)^{0.076} * (SP)^{2.767} * (F)^{-22.26} * (FL)^{1.604} * (FD)^{1.005}$$

$$* (A)^{-0.612} + 0.00013 * (C)^{-0.222} * \left(\frac{w}{b}\right)^{-0.491} * (SMS)^{0.587} * (S)^{1.496} * (SP)^{-0.109} * (F)^{0.878} * (FL)^{-0.153}$$

$$* (FD)^{0.021} * (A)^{-0.164} * (FA)^{-0.529} \tag{15}$$

The R^2, RMSE, and MAE measured using this model were 0.68, 1.05%, and 0.83%. The OBJ and SI values of the training dataset were 1.19% and 0.33, respectively.

5.3 MLR Model

The comparison of actual and predicted TSC of ECC with fly ash for both training and testing datasets, derived from earlier studies, is illustrated in Figs. 8a and 8b. Based on previous research data presented in Table 1, content is the primary factor affecting the TCS of ECC mixtures with fly ash. The MLR model with varying parameters can be utilized to predict the TSC of ECC containing fly ash.

$$TSC = 0.00012 * (C)^{-0.216} * (FA)^{-0.525} * (\frac{w}{b})^{-0.502} * (SMS)^{0.582} * (S)^{1.498} * (SP)^{-0.11} * (F)^{0.925}$$

$$* (FL)^{-0.145} * (FD)^{-0.029} * (A)^{-0.164} \tag{16}$$

The R^2, RMSE, and MAE measured using this model were 0.67, 1.07% and 0.84%. The OBJ and SI values of the training dataset were 1.21% and 3.34, respectively.
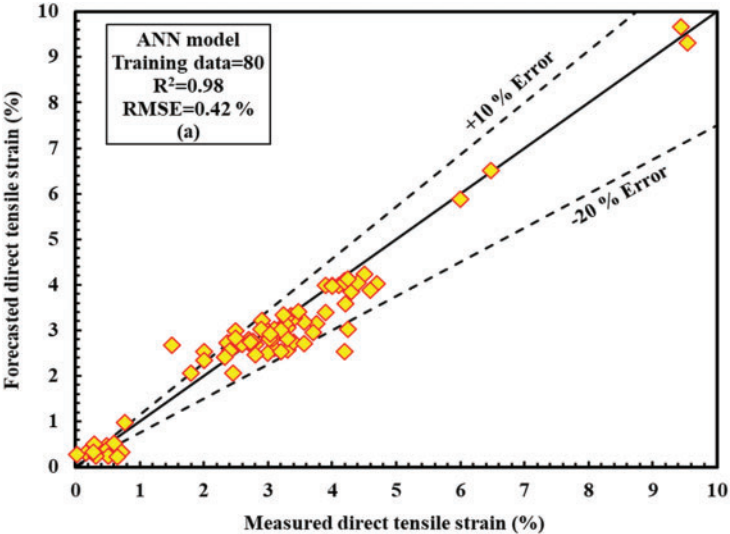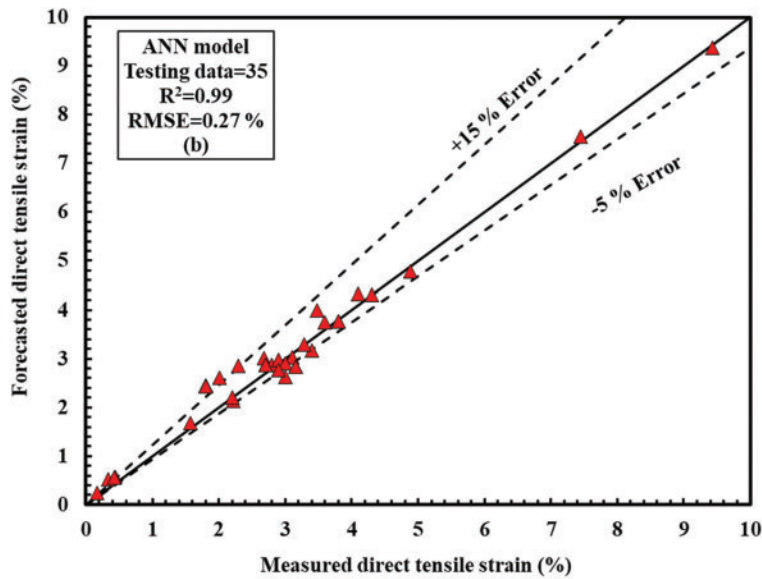

Figure 8: (Continued)

Figure 8: Comparison of the TSC of ECC mixtures that were tested and the TSC that the MLR model predicted; (a) training datasets; (b) testing datasets

5.4 ANN Model

Various hidden layers, neurons, momentum, learning rate, and iterations were explored to identify the ANN with the highest efficiency, as depicted in Fig. 5. The investigation determined that the CS of ECC with fly ash is best predicted when the ANN includes one hidden layer, seven neurons per side (Fig. 9), 2000 iterations, a 0.2 learning rate, and 0.1 momentum. The predicted and measured TSC of ECC containing fly ash for training and testing datasets are shown in Figs. 9a and 9b. The training datasets exhibited +10% and −20% error lines, while testing datasets showed +15% and −5% error lines, indicating superior performance compared to other proposed models.

Figure 9: (Continued)

Figure 9: Comparison of the TSC of ECC mixtures that were tested and the TSC that the ANN model predicted; (a) training datasets; (b) testing datasets

The R², RMSE, and MAE measured using this model were 0.98, 0.42% and 0.30%. The OBJ and SI values of the training dataset were 0.33% and 0.135, respectively.

5.5 M5P Model

The actual and predicted TSC of ECC mixtures with fly ash for both training and testing datasets are demonstrated in Figs. 10a and 10b. The TSC of ECC mixtures containing fly ash is notably affected by the w/b ratio, consistent with other investigated models and in line with empirical data in Table 1. Moreover, Eq. (17) represents the model with variables chosen based on the tree regression function.

$$TSC = -4.9043 - 0.0015\,(FA) - 4.6679\left(\frac{w}{b}\right) + 0.0026\,(SMS) + 0.0092\,(S) - 0.0573\,(SP)$$

$$+\, 0.1034\,(F) + 0.0916\,(FD)$$

The assessment parameters R², RMSE, and MAE for this model were 0.85, 0.98%, and 0.73%, respectively, and the OBJ and SI values of the training dataset were 0.78% and 0.314.

5.6 Model Comparisons

The precision of each model in predicting the tensile strain capacity of ECC was assessed using the statistical indices listed in Section 4.5. The ANN model has a higher R² and lower RMSE and MAE values when compared to the LR, NLR, MLR, and M5P models, as demonstrated in Figs. 11–13 for R² values, RMSE, and MAE, respectively. Fig. 14 compares model TSC estimations based on testing datasets for ECC mixes, including fly ash. Fig. 15 also displays the residual error for all models using training and testing datasets. In both Figs. 14 and 15, the estimated and predicted results of TSC for the ANN model are closer, demonstrating that the ANN model outperforms other models.
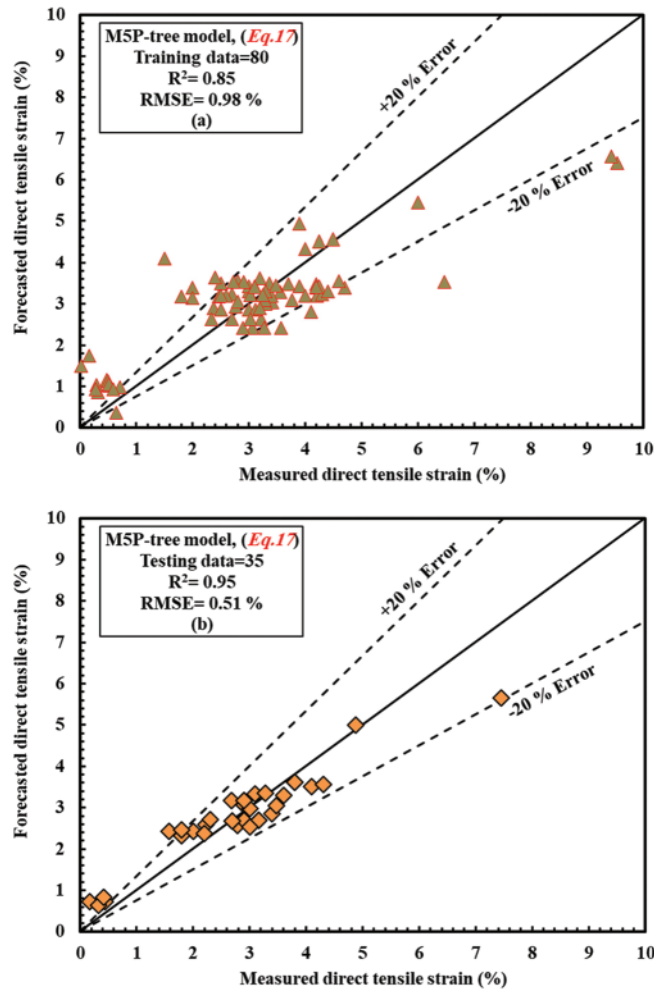
Figure 10: Comparison of the TSC of ECC mixtures that were tested and the DTS that the M5P model predicted; (a) training datasets; (b) testing datasets
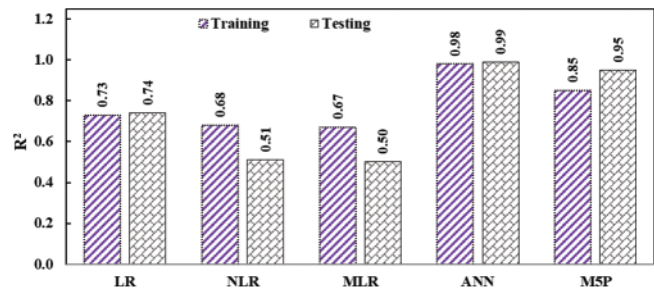

Figure 11: R^2 results for training and testing datasets for various proposed models

The OBJ values for all developed models are shown in Fig. 16. The LR, NLR, MLR, M5P, and ANN models have 0.94%, 1.19%, 1.21%, 0.78%, and 0.33%, respectively. The ANN model had an OBJ value 226% less than that of the NLR and MLR models; it is also 184% less than the LR model and

136% lower than the M5P model. This indicates that the ANN approach is more robust in forecasting the TSC of ECC mixes, including FA.
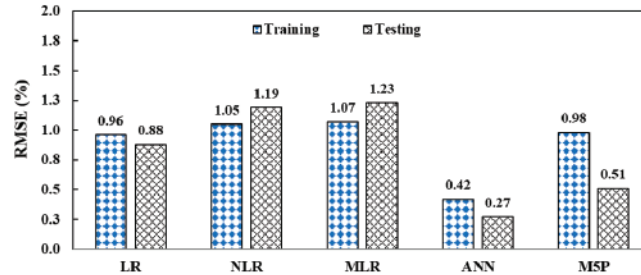
Figure 12: RMSE results for training and testing datasets for various proposed models
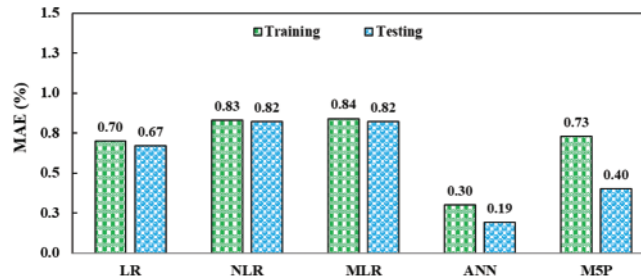
Figure 13: MAE results for training and testing datasets for various proposed models
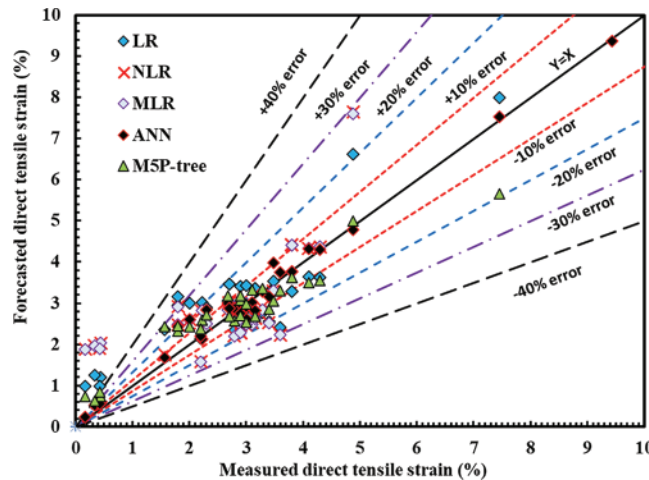
Figure 14: Comparison of model predictions of the TSC of ECC mixtures with data from the test datasets

The SI values for the given models are presented in Fig. 17 throughout the training and testing processes. Fig. 17 suggests that, except for the ANN model, the SI values for all phases were higher than 0.3, indicating poor performance. The SI training dataset values for the ANN model, however, were between 0.1 and 0.2, indicating that the ANN model performed well. Moreover, consistent with other performance measures, the ANN model has lower SI values than other methods. In the training

phase, the ANN model has a 128% lower SI value than the LR model and a 226% lower SI value in the testing phase. Additionally, compared to the NLR and MLR models, the ANN model had lower SI values in all stages, such as 152% lower in training and 344% lower in the testing stage. This further illustrates that the ANN model is more proficient and precise in predicting the TSC of ECC mixes, including FA, than the LR, NLR, M5P, and MLR models.
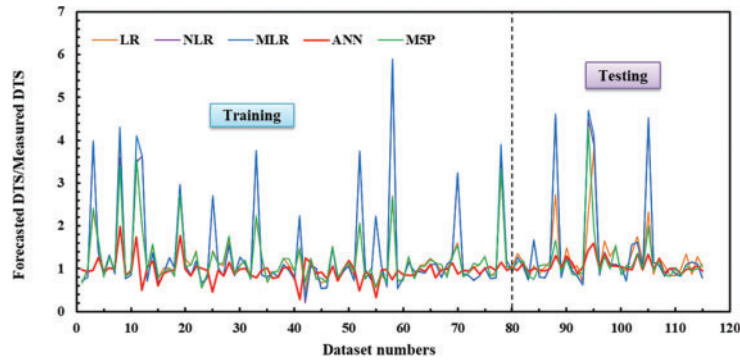

Figure 15: TSC of ECC mixes residual error diagram utilizing entire datasets for all models
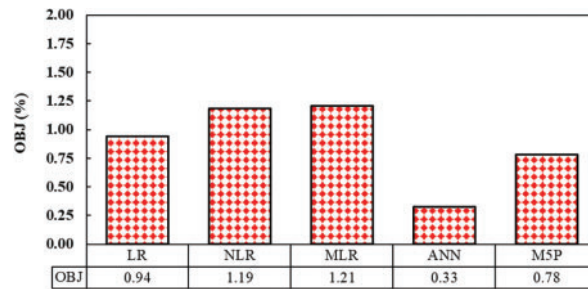
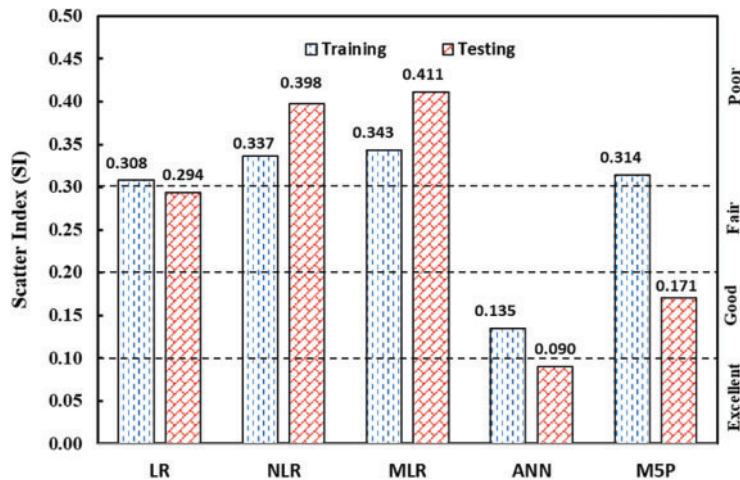**Figure 16:** All of the models' OBJ values

Figure 17: SI performance parameter results of several created models

6 Conclusions

Models for tensile strain capacity prediction that are precise and accurate can save time and money. The following conclusions were drawn based on a study and simulation of data from prior research to predict the TSC of ECC for 115 different mixed compositions:

1. In the production of ECC mixes, the range of some ingredients falls within a narrow range of available input space. This phenomenon is attributed to the special mix proportion of this concrete type. Therefore, the application of the proposed models should be verified for mix proportions outside the ranges provided in this study.

2. The mixture proportion and quality of materials are crucial in producing ECC because the TSC is highly sensitive to the amount and quality of materials.

3. Among various models developed to predict the TSC of ECC mixtures, the ANN model outperformed other models in all phases based on different assessment criteria, with higher R^2 values, lower OBJ values, lower RMSE, lower SI, and lower MAE values.

4. Except for the ANN model, the SI values for all models and stages exceeded 0.3, suggesting suboptimal performance.

5. The SI value for the ANN model in the training phase ranged between 0.1 and 0.2, indicating good performance; for the testing phase, the value ranged from 0 to 0.1, suggesting that the ANN model performed exceptionally well.

6. The OBJ value of the ANN model is 226% lower than those of the NLR and MLR models; it is also 184% lower than that of the LR model and 135% lower than the M5P model. This demonstrates that the ANN model is more accurate and adept at forecasting the TSC of ECC mixes, including F.

7. The overall findings and analysis revealed that specific quantities of FA can be effectively utilized in ECC production to produce sustainable, environmentally friendly, and structurally sound ECCs. Furthermore, the models developed in this study, especially the ANN model, can efficiently estimate the mix proportions and TSC of ECCs, thereby reducing the number of experimental tests and trial batches in the laboratory.

Author Contributions: The authors confirm their contribution to the paper as follows: study conception and design: Rabar H. Faraj, Hemn Unis Ahmed, and Hardi Saadullah Fathullah; data collection: Rabar H. Faraj, Hemn Unis Ahmed, and Alan Saeed; analysis and interpretation of results: Rabar H. Faraj and Hemn Unis Ahmed; draft manuscript preparation: Hardi Saadullah Fathullah, Alan Saeed Abdulrahman and Farid Abed. All authors reviewed the results and approved the final version of the manuscript.

Availability of Data and Materials: All the data are available in the paper.

Conflicts of Interest: The authors declare that they have no conflicts of interest to report regarding the present study.

References

1. Li, V. C. (1992). Performance driven design of fiber reinforced cementitious composites. *Proceedings of 4th RILEM International Symposium on Fiber Reinforced Concrete*, University of Sheffield.

2. Li, V. C. (1992). Postcrack scaling relations for fiber reinforced cementitious composites. *Journal of Materials in Civil Engineering, 4(1),* 41–57. https://doi.org/10.1061/10.1061/(ASCE)0733-9399(1992)118:11(2246)

3. Li, V. C., Leung, C. K. (1992). Steady-state and multiple cracking of short random fiber composites. *Journal of Engineering Mechanics, 118(11),* 2246–2264. https://doi.org/10.1061/(ASCE)0733-9399(1992)118:11(2246)

4. Li, V. C., Wu, H. C. (1992). Conditions for pseudo strain-hardening in fiber reinforced brittle matrix composites. *Applied Mechanics Reviews, 45(8),* 390–398.

5. Li, V. C., Wang, S., Wu, C. (2001). Tensile strain-hardening behavior of polyvinyl alcohol engineered cementitious composite (PVA-ECC). *Materials Journal, 98(6),* 483–492.

6. Lim, Y. M., Li, V. C. (1997). Durable repair of aged infrastructures using trapping mechanism of engineered cementitious composites. *Cement and Concrete Composites, 19(4),* 373–385. https://doi.org/10.1016/S0958-9465(97)00026-7

7. Şahmaran, M., Al-Emam, M., Yıldırım, G., Şimşek, Y. E., Erdem, T. K. et al. (2015). High-early-strength ductile cementitious composites with characteristics of low early-age shrinkage for repair of infrastructures. *Materials and Structures, 48(5),* 1389–1403. https://doi.org/10.1617/s11527-013-0241-z

8. Maalej, M., Quek, S. T., Ahmed, S. F. U., Zhang, J., Lin, V. W. J. et al. (2012). Review of potential structural applications of hybrid fiber engineered cementitious composites. *Construction and Building Materials, 36,* 216–227. https://doi.org/10.1016/j.conbuildmat.2012.04.010

9. Qudah, S., Maalej, M. (2014). Application of engineered cementitious composites (ECC) in interior beam-column connections for enhanced seismic resistance. *Engineering Structures, 69,* 235–245. https://doi.org/10.1016/j.engstruct.2014.03.026

10. Pan, Z., Wu, C., Liu, J., Wang, W., Liu, J. (2015). Study on mechanical properties of cost-effective polyvinyl alcohol engineered cementitious composites (PVA-ECC). *Construction and Building Materials, 78,* 397–404. https://doi.org/10.1016/j.conbuildmat.2014.12.071

11. Li, L. Z., Bai, Y., Yu, K. Q., Yu, J. T., Lu, Z. D. (2019). Reinforced high-strength engineered cementitious composite (ECC) columns under eccentric compression: Experiment and theoretical model. *Engineering Structures, 198,* 109541. https://doi.org/10.1016/j.engstruct.2019.109541

12. Yang, E. H., Li, V. C. (2010). Strain-hardening fiber cement optimization and component tailoring by means of a micromechanical model. *Construction and Building Materials, 24(2),* 130–139. https://doi.org/10.1016/j.conbuildmat.2007.05.014

13. Madhavi, K. B., Venugopal, M., Rajesh, V., Suresh, K. (2016). Experimental study on bendable concrete. *International Journal of Engineering Research & Technology, 5(10),* 501–550.

14. Neville, A. M., Brooks, J. J. (1987). *Concrete technology*, pp. 242–246. England: Longmann Scientific & Technical.

15. Neville, A. M. (1995). *Properties of concrete*. London: Longman.

16. Gupta, S., Sihag, P. (2022). Prediction of the compressive strength of concrete using various predictive modeling techniques. *Neural Computing and Applications,* 1–11. https://doi.org/10.1007/s00521-021-06820-y

17. Shariati, M., Mafipour, M. S., Ghahremani, B., Azarhomayun, F., Ahmadi, M. et al. (2020). A novel hybrid extreme learning machine-grey wolf optimizer (ELM-GWO) model to predict compressive strength of concrete with partial replacements for cement. *Engineering with Computers,* 1–23. https://doi.org/10.1007/s00366-020-01081-0

18. Skentou, A. D., Bardhan, A., Mamou, A., Lemonis, M. E., Kumar, G. et al. (2022). Closed-form equation for estimating unconfined compressive strength of granite from three non-destructive tests using soft computing models. *Rock Mechanics and Rock Engineering, 56,* 487–514. https://doi.org/10.1007/s00603-022-03046-9

19. Emad, W., Mohammed, A. S., Kurda, R., Ghafor, K., Cavaleri, L. et al. (2022). Prediction of concrete materials compressive strength using surrogate models. *Structures, 46,* 1243–1267. Elsevier. https://doi.org/10.1016/j.istruc.2022.11.002

20. Aggarwal, S., Bhargava, G., Sihag, P. (2021). Prediction of compressive strength of SCC-containing metakaolin and rice husk ash using machine learning algorithms. In: *Computational technologies in materials science*, pp. 193–205. Tyler and Francis: CRC Press.

21. Gao, W., Karbasi, M., Derakhsh, A. M., Jalili, A. (2019). Development of a novel soft-computing framework for the simulation aims: A case study. *Engineering with Computers, 35(1),* 315–322. https://doi.org/10.1007/s00366-018-0601-y

22. Almohammed, F., Sihag, P., Sammen, S. S., Ostrowski, K. A., Singh, K. et al. (2022). Assessment of soft computing techniques for the prediction of compressive strength of bacterial concrete. *Materials, 15(2),* 489. https://doi.org/10.3390/ma15020489

23. Cavaleri, L., Barkhordari, M. S., Repapis, C. C., Armaghani, D. J., Ulrikh, D. V. et al. (2022). Convolution-based ensemble learning algorithms to estimate the bond strength of the corroded reinforced concrete. *Construction and Building Materials, 359,* 129504. https://doi.org/10.1016/j.conbuildmat.2022.129504

24. Behnood, A., Daneshvar, D. (2020). A machine learning study of the dynamic modulus of asphalt concretes: An application of M5P model tree algorithm. *Construction and Building Materials, 262,* 120544. https://doi.org/10.1016/j.conbuildmat.2020.120544

25. Ahmed, H. U., Mohammed, A. S., Mohammed, A. A., Faraj, R. H. (2021). Systematic multiscale models to predict the compressive strength of fly ash-based geopolymer concrete at various mixture proportions and curing regimes. *PLoS One, 16(6),* e0253006. https://doi.org/10.1371/journal.pone.0253006

26. Uddin, M. N., Li, L. Z., Ahmed, A., Almajhali, K. Y. M. (2022). Prediction of PVA fiber effect in engineered composite cement (ECC) by artificial neural network (ANN). *Materials Today: Proceedings, 65,* 537–542. https://doi.org/10.1016/j.matpr.2022.03.088

27. Alaloul, W. S., Musarat, M. A., Haruna, S., Tayeh, B. A., Norizan, M. N. B. (2022). Chemical attack on concrete containing a high volume of crumb rubber as a partial replacement for fine aggregate in engineered cementitious composite (ECC). *Canadian Journal of Civil Engineering, 49(1),* 11–17. https://doi.org/10.1139/cjce-2020-0343

28. Qadir, W., Ghafor, K., Mohammed, A. (2019). Characterizing and modeling the mechanical properties of the cement mortar modified with fly ash for various water-to-cement ratios and curing times. *Advances in Civil Engineering, 2019,* 7013908. https://doi.org/10.1155/2019/7013908

29. Huang, X., Ranade, R., Ni, W., Li, V. C. (2013). Development of green engineered cementitious composites using iron ore tailings as aggregates. *Construction and Building Materials, 44,* 757–764. https://doi.org/10.1016/j.conbuildmat.2013.03.088

30. Huang, X., Ranade, R., Ni, W., Li, V. C. (2013). On the use of recycled tire rubber to develop low E-modulus ECC for durable concrete repairs. *Construction and Building Materials, 46,* 134–141. https://doi.org/10.1016/j.conbuildmat.2013.04.027

31. Meng, D., Lee, C. K., Zhang, Y. X. (2017). Flexural and shear behaviours of plain and reinforced polyvinyl alcohol-engineered cementitious composite beams. *Engineering Structures, 151,* 261–272. https://doi.org/10.1016/j.engstruct.2017.08.036

32. Soe, K. T., Zhang, Y. X., Zhang, L. C. (2013). Material properties of a new hybrid fibre-reinforced engineered cementitious composite. *Construction and Building Materials, 43,* 399–407. https://doi.org/10.1016/j.conbuildmat.2013.02.021

33. Yu, J., Lin, J., Zhang, Z., Li, V. C. (2015). Mechanical performance of ECC with high-volume fly ash after sub-elevated temperatures. *Construction and Building Materials, 99,* 82–89. https://doi.org/10.1016/j.conbuildmat.2015.09.002

34. Zhu, W., Bartos, P. J., Porro, A. (2004). Application of nanotechnology in construction. *Materials and Structures, 37(9),* 649–658. https://doi.org/10.1007/BF02483294

35. Liu, H., Zhang, Q., Gu, C., Su, H., Li, V. C. (2016). Influence of micro-cracking on the permeability of engineered cementitious composites. *Cement and Concrete Composites, 72,* 104–113. https://doi.org/10.1016/j.cemconcomp.2016.05.016

36. Liu, H., Zhang, Q., Li, V., Su, H., Gu, C. (2017). Durability study on engineered cementitious composites (ECC) under sulfate and chloride environment. *Construction and Building Materials, 133,* 171–181. https://doi.org/10.1016/j.conbuildmat.2016.12.074

37. Kan, L. L., Shi, R. X., Zhu, J. (2019). Effect of fineness and calcium content of fly ash on the mechanical properties of engineered cementitious composites (ECC). *Construction and Building Materials, 209,* 476–484. https://doi.org/10.1016/j.conbuildmat.2019.03.129

38. Lepech, M. D., Li, V. C. (2009). Water permeability of engineered cementitious composites. *Cement and Concrete Composites, 31(10),* 744–753. https://doi.org/10.1016/j.cemconcomp.2009.07.002

39. Qian, S. Z., Zhou, J., Schlangen, E. (2010). Influence of curing condition and precracking time on the self-healing behavior of engineered cementitious composites. *Cement and Concrete Composites, 32(9),* 686–693. https://doi.org/10.1016/j.cemconcomp.2010.07.015

40. Qian, S., Zhou, J., de Rooij, M. R., Schlangen, E., Ye, G. et al. (2009). Self-healing behavior of strain hardening cementitious composites incorporating local waste materials. *Cement and Concrete Composites, 31(9),* 613–621. https://doi.org/10.1016/j.cemconcomp.2009.03.003

41. Şahmaran, M., Li, V. C. (2008). Durability of mechanically loaded engineered cementitious composites under highly alkaline environments. *Cement and Concrete Composites, 30(2),* 72–81. https://doi.org/10.1016/j.cemconcomp.2007.09.004

42. Şahmaran, M., Li, V. C. (2009). Influence of microcracking on water absorption and sorptivity of ECC. *Materials and Structures, 42(5),* 593–603. https://doi.org/10.1617/s11527-008-9406-6

43. Şahmaran, M., Li, V. C. (2007). De-icing salt scaling resistance of mechanically loaded engineered cementitious composites. *Cement and Concrete Research, 37(7),* 1035–1046. https://doi.org/10.1016/j.cemconres.2007.04.001

44. Şahmaran, M., Li, V. C. (2009). Durability properties of micro-cracked ECC containing high volumes fly ash. *Cement and Concrete Research, 39(11),* 1033–1043. https://doi.org/10.1016/j.cemconres.2009.07.009

45. Sahmaran, M., Li, M., Li, V. C. (2007). Transport properties of engineered cementitious composites under chloride exposure. *ACI Materials Journal, 104(6),* 604–611.

46. Şahmaran, M., Lachemi, M., Hossain, K. M., Li, V. C. (2009). Internal curing of engineered cementitious composites for prevention of early age autogenous shrinkage cracking. *Cement and Concrete Research, 39(10),* 893–901. https://doi.org/10.1016/j.cemconres.2009.07.006

47. Sahmaran, M., Yücel, H. E., Demirhan, S., Artfytfk, M. T., Li, V. C. (2012). Combined effect of aggregate and mineral admixtures on tensile ductility of engineered cementitious composites. *ACI Materials Journal, 109(6),* 627–637.

48. Şahmaran, M., Özbay, E., Yücel, H. E., Lachemi, M., Li, V. C. (2012). Frost resistance and microstructure of engineered cementitious composites: Influence of fly ash and micro poly-vinyl-alcohol fiber. *Cement and Concrete Composites, 34(2),* 156–165. https://doi.org/10.1016/j.cemconcomp.2011.10.002

49. Yang, E. H., Yang, Y., Li, V. C. (2007). Use of high volumes of fly ash to improve ECC mechanical properties and material greenness. *ACI Materials Journal, 104(6),* 620–628.

50. Yao, Y., Zhu, Y., Yang, Y. (2012). Incorporation superabsorbent polymer (SAP) particles as controlling pre-existing flaws to improve the performance of engineered cementitious composites (ECC). *Construction and Building Materials, 28(1),* 139–145. https://doi.org/10.1016/j.conbuildmat.2011.08.032

51. Gencturk, B., Hosseini, F. (2015). Evaluation of reinforced concrete and reinforced engineered cementitious composite (ECC) members and structures using small-scale testing. *Canadian Journal of Civil Engineering, 42(3),* 164–177. https://doi.org/10.1139/cjce-2013-0445

52. Guan, X., Li, Y., Liu, T., Zhang, C., Li, H. et al. (2019). An economical ultra-high ductile engineered cementitious composite with large amount of coarse river sand. *Construction and Building Materials, 201,* 461–472. https://doi.org/10.1016/j.conbuildmat.2018.12.207

53. Meng, D., Huang, T., Zhang, Y. X., Lee, C. K. (2017). Mechanical behaviour of a polyvinyl alcohol fibre reinforced engineered cementitious composite (PVA-ECC) using local ingredients. *Construction and Building Materials, 141,* 259–270. https://doi.org/10.1016/j.conbuildmat.2017.02.158

54. Zain, M. F. M., Abd, S. M. (2009). Multiple regression model for compressive strength prediction of high: Performance concrete. *Journal of Applied Sciences, 9,* 155–160. https://doi.org/10.3923/jas.2009.155.160

55. Demircan, E., Harendra, S., Vipulanandan, C. (2011). Artificial neural network and nonlinear models for gelling time and maximum curing temperature rise in polymer grouts. *Journal of Materials in Civil Engineering, 23(4),* 372–377. https://doi.org/10.1061/(ASCE)MT.1943-5533.0000172

56. Sarwar, W., Ghafor, K., Mohammed, A. (2019). Modeling the rheological properties with shear stress limit and compressive strength of ordinary Portland cement modified with polymers. *Journal of Building Pathology and Rehabilitation, 4(1),* 25. https://doi.org/10.1007/s41024-019-0064-6

57. Ahmed, H. U., Mohammed, A. S., Faraj, R. H., Qaidi, S. M., Mohammed, A. A. (2022). Compressive strength of geopolymer concrete modified with nano-silica: Experimental and modeling investigations. *Case Studies in Construction Materials, 16,* e01036. https://doi.org/10.1016/j.cscm.2022.e01036

58. Faraj, R. H., Ahmed, H. U., Rafiq, S., Sor, N. H., Ibrahim, D. F. et al. (2022). Performance of self-compacting mortars modified with nanoparticles: A systematic review and modeling. *Cleaner Materials,* 100086. https://doi.org/10.1016/j.clema.2022.100086

59. Hall, M., Frank, E., Holmes, G., Pfahringer, B., Reutemann, P. et al. (2009). The WEKA data mining software: An update. *ACM SIGKDD Explorations Newsletter, 11(1),* 10–18.

60. Sihag, P., Jain, P., Kumar, M. (2018). Modelling of impact of water quality on recharging rate of storm water filter system using various kernel function based regression. *Modeling Earth Systems and Environment, 4(1),* 61–68. https://doi.org/10.1007/s40808-017-0410-0

61. Faraj, R. H., Mohammed, A. A., Omer, K. M., Ahmed, H. U. (2022). Soft computing techniques to predict the compressive strength of green self-compacting concrete incorporating recycled plastic aggregates and industrial waste ashes. *Clean Technologies and Environmental Policy.* https://doi.org/10.1007/s10098-022-02318-w

62. Faraj, R. H., Mohammed, A. A., Mohammed, A., Omer, K. M., Ahmed, H. U. (2021). Systematic multiscale models to predict the compressive strength of self-compacting concretes modified with nanosilica at different curing ages. *Engineering with Computers,* 1–24. https://doi.org/10.1007/s00366-021-01385-9

63. Ahmed, H. U., Abdalla, A. A., Mohammed, A. S., Mohammed, A. A., Mosavi, A. (2022). Statistical methods for modeling the compressive strength of geopolymer mortar. *Materials, 15,* 1868. https://doi.org/10.3390/ma15051868

64. Quinlan, J. R. (1992). Learning with continuous classes. *5th Australian Joint Conference on Artificial Intelligence*, vol. 92, pp. 343–348. Perth, WA, Australia.

65. Malerba, D., Esposito, F., Ceci, M., Appice, A. (2004). Top-down induction of model trees with regression and splitting nodes. *IEEE Transactions on Pattern Analysis and Machine Intelligence, 26(5),* 612–625. https://doi.org/10.1109/TPAMI.2004.1273937

66. Li, M. F., Tang, X. P., Wu, W., Liu, H. B. (2013). General models for estimating daily global solar radiation for different solar radiation zones in mainland China. *Energy Conversion and Management, 70,* 139–148. https://doi.org/10.1016/j.enconman.2013.03.004

67. Golafshani, E. M., Behnood, A., Arashpour, M. (2020). Predicting the compressive strength of normal and High-Performance Concretes using ANN and ANFIS hybridized with Grey Wolf Optimizer. *Construction and Building Materials, 232,* 117266. https://doi.org/10.1016/j.conbuildmat.2019.117266